JVS

Neonatal influenza virus infection affects myelination in influenza-recovered mouse brain

Jin Hee Kim, Ji Eun Yu, Byung-Joon Chang, Sang-Soep Nahm*

Department of Veterinary Medicine, College of Veterinary Medicine, Konkuk University, Seoul 05029, Korea

Influenza virus infection is a zoonosis that has great socioeconomic effects worldwide. Influenza infection induces respiratory symptoms, while the influenza virus can infect brain and leave central nervous system sequelae. As children are more vulnerable to infection, they are at risk of long-term neurological effects once their brains are infected. We previously demonstrated that functional changes in hippocampal neurons were observed in mice recovered from neonatal influenza infection. In this study, we investigated changes in myelination properties that could affect neural dysfunction. Mice were infected with the influenza virus on postnatal day 5. Tissues were harvested from recovered mice 21-days post-infection. The expression levels for myelin basic protein (MBP) were determined, and immunohistochemical staining and transmission electron microscopy were performed. Real-time polymerase chain reaction and Western blot analyses showed that mRNA and protein expressions increased in the hippocampus and cerebellum of recovered mice. Increased MBP-staining signal was observed in the recovered mouse brain. By calculating the relative thickness of myelin sheath in relation to nerve fiber diameter (G-ratio) from electron photomicrographs, an increased G-ratio was observed in both the hippocampus and cerebellum of recovered mice. Influenza infection in oligodendrocyte-enriched primary brain cell cultures showed that proinflammatory cytokines may induce MBP upregulation. These results suggested that increased MBP expression could be a compensatory change related to hypomyelination, which may underlie neural dysfunction in recovered mice. In summary, the present results demonstrate that influenza infection during the neonatal period affects myelination and further induces functional changes in influenza-recovered mouse brain.

Keywords: cerebellum, hippocampus, influenza, myelin, oligodendrocyte

Introduction

Influenza virus infection is a zoonosis and considered a significant risk to human and animal health. A recent study on the 2009 global influenza A (H1N1) pandemic reported high morbidity/mortality, which had a great socioeconomic impact worldwide [30]. Influenza infection causes medical burden in children, elderly people, and people with chronic medical conditions. Specifically, high mortality is obvious in elderly people and high morbidity has been reported in children less than five years old [31].

In general, influenza virus infection occurs via the respiratory tract and primarily results in acute respiratory symptoms. However, many reports indicate that the influenza virus can infect the central nervous system (CNS). Clinical cases involving influenza infection in the CNS among children are not rare [8]. Clinical symptoms among children include encephalopathy, seizures, and neurological complications such

as movement disorders [9,29,33,35]. These clinical case reports provide information related to the acute phase in the progress of the disease, which is caused by the influenza virus infection in the brain. A previous review paper described the long-term effects of influenza brain infection from historical influenza pandemics. It is interesting to note that after the influenza pandemic that occurred from 1916 to 1927, long-lasting behavioral disturbances were observed in children after the recovery period [15]. These changes included increased locomotion, sleep disturbance, mood change, and language disability. Recently, similar findings indicating that children who recovered from the 2009 influenza pandemic exhibited residual neurological sequelae were reported [1]. All these reports suggest that influenza infection may cause long-lasting neurological dysfunction and/or psychiatric disorders in children who recover from influenza infection in the brain.

While the progression of influenza infection in the acute phase is well known, the sequelae of influenza infection in the

CNS has not been reported. We previously reported that experimental influenza infection with a half-lethal dose in neonatal mice produced a suitable model for studies into the long-term effects of influenza infection in the CNS [31]. The infected mice showed a wide range of brain areas infected with the influenza virus during the peak infection period, and increased proinflammatory cytokine expression was associated with the infection. The recovered mice also exhibited functional changes in hippocampal neurons, which were characterized by noticeable deficits at rest and severe failures in neural conduction during higher activity [22].

The aim of this study is to investigate the mechanisms underlying neural dysfunction in recovered mice. Several studies have demonstrated that maternal influenza infection can alter the expression of myelination-related genes in offspring [6,7]. Our preliminary microarray study using influenza-recovered mice also demonstrated that several genes related to myelination were differentially regulated. Therefore, we investigated the expression of myelin basic protein (MBP) and the morphological characteristics of the myelin sheath in the hippocampus and cerebellum of recovered mice. Specifically, we adopted the concept of a G-ratio, which defines the relative thickness of a myelin sheath in relation to its axonal diameter [2]. By using the G-ratio, it was possible to characterize the properties of the myelin sheath in a quantitative manner; in addition, its ultrastructure was examined by using transmission electron microscopy.

Materials and Methods

Experimental animals

Five-day-old male and female BALB/c mice (Orient Bio, Korea) were used for all experiments described below. Influenza virus infection was performed in the animal biosafety level II facility at Konkuk University, Korea. The contents and methods of the animal experiments were approved by the institutional animal care and use committee at Konkuk University (KU16131).

Virus infection and tissue harvesting

In order to obtain mice that had recovered from influenza virus infection, mice were infected with the influenza virus at a half-lethal dose (30 μL of 10^3 TCID$_{50}$/mL; TCID, 50% tissue culture infectious dose) as previously described [34]. Animals were injected intraperitoneally either with influenza A virus (A/NWS/33 H1N1; provided by Dr. Song, College of Veterinary Medicine, Konkuk University) or a same volume of saline as a control. Hippocampal and cerebellar tissue samples were collected on day 21 post-infection, which is the time point when the viral infection is resolved, based on the absence of viral antigen detection by real-time polymerase chain reaction (RT-PCR) on this day [34]. For each experiment, three to five control and recovered mice were used.

RT-PCR

Total RNA was extracted from the hippocampus, cerebellum (n = 5 per group), or oligodendrocyte precursor cell (OPC) culture (n = 5 per group) by using TRIzol reagent (Invitrogen, USA). The cDNAs were synthesized with 5 μg of total RNA by using the Superscript first-strand synthesis system for RT-PCR (Invitrogen) and stored at −20°C. To quantitatively analyze the expression level of *MBP*, the PCR was performed using SYBR Green Premix Ex Taq II Kit (Takara Bio, Japan) in a CHROMO4 (Bio-Rad Laboratories, USA) RT-PCR system. The PCR was allowed to proceed for 40 cycles. The results were analyzed using CFX Manager software (Bio-Rad Laboratories), and the relative expression levels were normalized in relation to the expression of glyceraldehyde 3-phosphate dehydrogenase (GAPDH), according to the manufacturer's instructions. The specific primer sequences for the detection of *MBP*, *interleukin-6* (*IL-6*), *interleukin-1β* (*IL-1β*), *tumor necrosis factor-α* (*TNF-α*), and *GAPDH* are shown in Table 1 [34].

Western blot analysis

MBP expression was compared between control and recovered mice by assessing Western blot. Total protein was extracted separately from the hippocampus and cerebellum (n = 4 per group) using T-PER tissue protein extraction buffer

Table 1. Sequences of primers used in real-time polymerase chain reaction

Gene	Forward sequence	Reverse sequence
MBP	CCG AGA ACA TAC CAG AGA ATC	CAC TTA CAC TTC AGA CAC AGA
IL-6	TTC ACC ATG GAG AAG GC	GGC ATG GAC TGT GGT CAT GA
IL-1β	GAC CTT CCA GGA TGA GGA CA	AGG CCA CAG GTA TTT TGT CG
TNF-α	CCG ATG GGT TGT ACC TTG TC	CGG ACT CCG CAA AGT CTA AG
GAPDH	TTC ACC ATG GAG AAG GC	GGC ATG GAC TGT GGT CAT GA

MBP, myelin basic protein; IL-1β, interleukin-1β; IL-6, interleukin-6; TNF-α, tumor necrosis factor-α; GAPDH, glyceraldehyde 3-phosphate dehydrogenase.

(Pierce, USA). The concentration of the extracted protein was measured using a BCA protein assay kit (Pierce). Proteins were subjected to SDS-PAGE, followed by electrotransfer to PVDF membranes (Millipore, USA). Protein-transferred membranes were blocked with 5% skim milk in 0.1% Tris-buffered saline/Tween-20. The blots were probed with a primary antibody against MBP (1:1,000; Millipore), overnight at 4°C. β-Actin was used as a loading control (1:10,000; Sigma-Aldrich, USA). After incubation, the membranes were subsequently incubated for 2 h at room temperature with the appropriate secondary antibodies conjugated with horseradish peroxidase (Vector, USA). The protein bands were visualized with SuperSignal West Pico Chemiluminescent Substrate (Pierce). The bands were captured and intensity quantification followed by using the Luminescent Image Analyzer System LAS 4000 with image analysis software (Fuji, USA).

Immunohistochemistry

Control and recovered mice (n = 3 per group) were anesthetized by intraperitoneal injection of tribromoethanol (250 mg/kg; Sigma-Aldrich). The animals were transcardially perfused with phosphate-buffered saline (PBS) to remove blood in the brain, and further perfused with 4% paraformaldehyde for fixation. The brains were removed and post-fixed in the same fixative overnight at 4°C. The fixed brain was cut along the mid-sagittal plane, and the tissue was processed for routine paraffin embedding. The paraffin-embedded mouse brain was sectioned at 4 μm thickness for immunohistochemical analysis. Briefly, the sections were hydrated, quenched with 0.3% hydrogen peroxide in methanol, and subsequently blocked with 5% equine serum in PBS for 1 h at room temperature. The sections were incubated with the antibody against MBP (1:1,000; Millipore), overnight at 4°C. The sections were then incubated with biotinylated anti-rat IgG (Vector) for 2 h at room temperature and subsequently with horseradish peroxidase-conjugated streptavidin (Vector) for 1 h at room temperature. The signal was visualized using diaminobenzidine as a substrate and counterstained with methyl green. The stained slides were dehydrated, mounted, and evaluated with a light microscope (Olympus, Japan). Negative control staining was carried out by omitting the primary antibody to ensure antibody specificity to MBP. Optical density was measured equally for the hippocampal molecular layer and the cerebellar white matter from five tissue sections per animal. ImageJ software (ver. 1.48; National Institutes of Health, USA) was used to measure optical density by manually outlining the designated stained areas.

Transmission electron microscopy and image analysis

Control and recovered mice (n = 3 per group) were anesthetized as previously described. They were then perfused with 4% paraformaldehyde and 1% glutaraldehyde in phosphate buffer. In order to acquire tissues from the same locations, 1 mm thick sections of removed brains were obtained using a sagittal and coronal mouse brain slicer matrix (Zivic, USA). The sectioned tissues were post-fixed in 2.5% glutaraldehyde buffer at 4°C overnight. The tissue sections were osmicated with 2% osmium tetroxide for 2 h at room temperature. After repeated rinsing and stepwise dehydration, tissues were embedded in an epoxy mix, then cured at 60°C for 48 h. Ultrathin sections were made using an ultra-microtome (EM UC7; Leica, Germany). The sections were stained with uranyl acetate, then with lead citrate for 10 min. Electron microscopic images were obtained using a transmission electron microscope (JEM 1010; JEOL, Japan). At least 10 electron microscopic images were obtained from the hippocampus and cerebellum of each animal for image analysis.

In order to determine the relative thickness of the myelin sheath in a quantitative manner, the G-ratio was calculated. Briefly, the G-ratio was obtained by following a previously described procedure [3]. With ImageJ software, the grayscale electron microscopic images were converted to black and white images. A threshold was applied to these images only to reveal the area occupied by the myelin sheath. First, the area occupied by the myelin sheath was calculated, then the area occupied by fibers was manually filled for calculation. Finally, the axonal radius (r) and the radius of the nerve fiber that includes the axon and myelin sheath (R) were obtained for calculation of the G-ratio (r/R).

OPC culture

OPCs were cultured to investigate the relationship between influenza infection and myelin expression. OPCs were isolated using the Papain Dissociation System (Worthington, USA) according to the manufacturer's instructions. Briefly, brains from 1-day-old animals were immediately removed and washed in a tube containing cold HBSS buffer followed by incubation at 37°C for 5 min. Brain tissue was dissociated by incubation with papain at 37°C, followed by trituration. Dissociated cells were pelleted and then resuspended in a medium with ovomucoid. The cells were passed through a nylon mesh strainer and were cultured for subsequent experiments. Fluorescence-activated cell sorting (FACS) was performed to verify the ratio of oligodendrocytes in primary brain cell cultures using an O4 antibody (Miltenyi Biotec, Germany) in a cell analyzer (FACSCalibur; BD Biosciences, USA). Cell viability was determined at 6, 12, 24, and 48 h post-infection by using a trypan blue exclusion assay.

Statistics

All data obtained from control and recovered mice were statistically analyzed using the Student's *t*-test. Data are

presented as mean ± SEM.

Results

MBP RT-PCR

MBP expression levels in the hippocampus and cerebellum of control and recovered mice were determined by quantitative RT-PCR. The mRNA levels of MBP in the hippocampus and cerebellum increased by 1.41 and 1.52 folds, respectively ($p < 0.05$; Fig. 1).

MBP Western blot

Protein expression for MBP in the hippocampus and cerebellum of control and recovered mice were quantitatively analyzed via Western blot analysis. MBP expression significantly increased both in the hippocampus ($p < 0.05$) and cerebellum ($p < 0.01$) of the recovered mice (Fig. 2). The tendency for an increase in MBP expression was similar to that for mRNA expression as both protein and mRNA expressions were higher in the cerebellum than in the hippocampus.

MBP immunohistochemistry

The morphological characteristics of MBP expression were assessed by immunohistochemical staining. We stained sections in the same batch to ensure all sections were exposed to the same staining condition. As MBP is a major constituent of the myelin sheath, positive staining signals are localized to the white matter. Within the hippocampus, MBP signals were localized to the molecular layer around Cornu Ammonis (CA)1 and CA2. MBP signals in the cerebellum were mostly obvious within the cerebellar white matter. In general, this immunohistochemical staining technique is not intended for quantitative analysis; however, densitometric analysis was
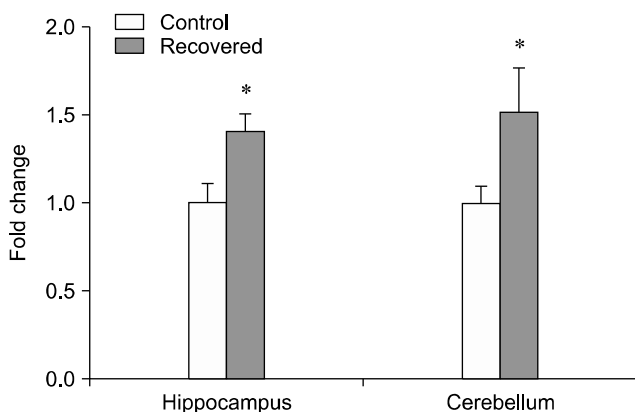
performed for semi-quantitative examination. More intense MBP signals were observed in the recovered mouse cerebellum, while the signals in the recovered mouse hippocampus showed a tendency toward an increase ($p < 0.07$) that did not reach statistical significance (Fig. 3).

Transmission electron microscopy and the G-ratio

Transmission electron microscopy revealed the fine structure of the myelin sheaths in the hippocampus and cerebellum. The myelin sheath was easily identified from cross-sectioned axons. The general appearance of myelin sheaths around axons was comparable between control and recovered mice brains and the thickness was variable. No specific differences in morphological characteristics were noticed (Fig. 4).

To explore morphological properties of the myelin sheath in a quantitative manner in association with increased MBP mRNA and protein expression in the recovered mouse brain, the G-ratio was calculated to evaluate the thickness of the myelin sheath relative to the axonal radius. A stepwise image processing procedure enabled us to determine the area of individual myelin sheath to axon ratio. The results obtained from image analyses revealed that the G-ratios for the recovered mouse significantly increased by 6% in the hippocampus and by
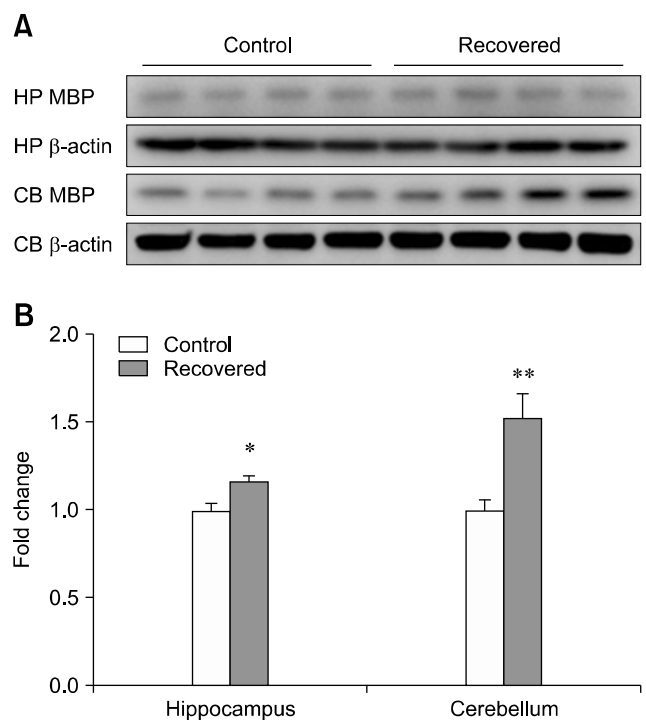

Fig. 1. Real-time polymerase chain reaction analysis of *myelin basic protein* (*MBP*) expression in the hippocampus and cerebellum of control and influenza-recovered mice. *MBP* expression in recovered mice was significantly increased both in the hippocampus and cerebellum (n = 5; *$p < 0.05$).

Fig. 2. Representative images (A) and quantification data from Western blot analyses for myelin basic protein (MBP) expression in the hippocampus (HP) and cerebellum (CB) of control and recovered mice (B). MBP expression in recovered mice was significantly increased both in the hippocampus and cerebellum (n = 4; *$p < 0.05$, **$p < 0.01$).
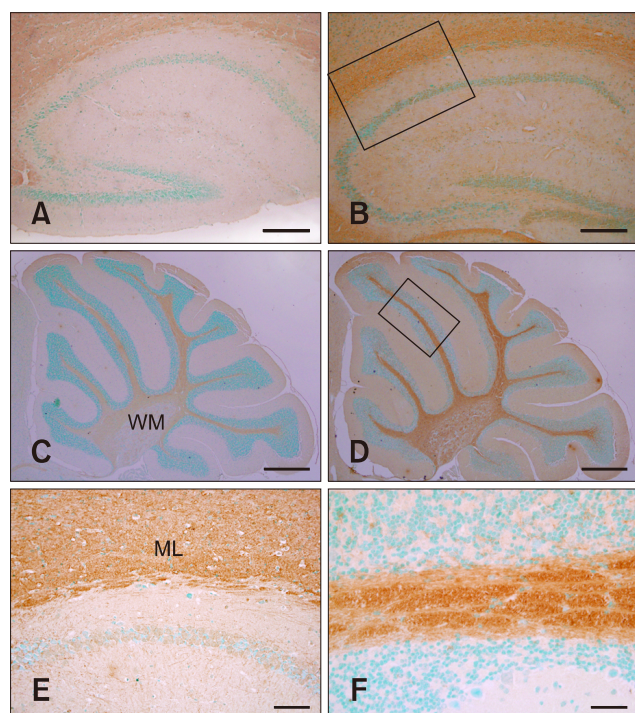
Fig. 3. Representative photomicrographs of myelin basic protein (MBP) immunohistochemical staining in the hippocampus and cerebellum of control (A and C) and recovered (B, D–F) mice. Positive staining for MBP expression was detected in the molecular layer (ML) of the hippocampus and in the white matter (WM) of the cerebellum. High magnification images of the indicated fields in the hippocampus (B) and the cerebellum (D) are shown in panels E and F in Fig. 3, respectively. The optical density measured from the stained areas was significantly higher in the cerebellar WM in recovered mice (G; $*p < 0.05$). Scale bars = 200 μm (A and B), 50 μm (C–E), 100 μm (F).
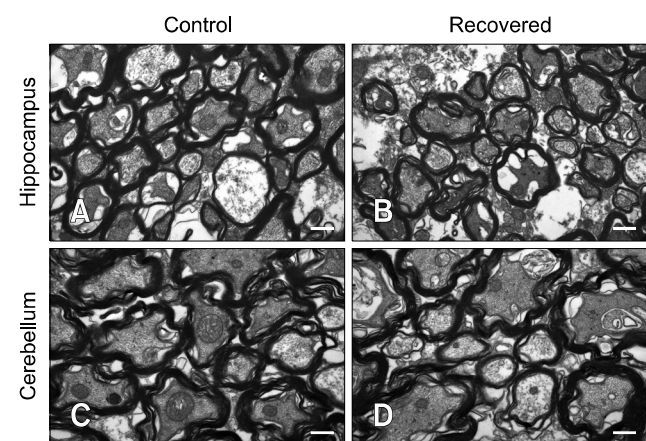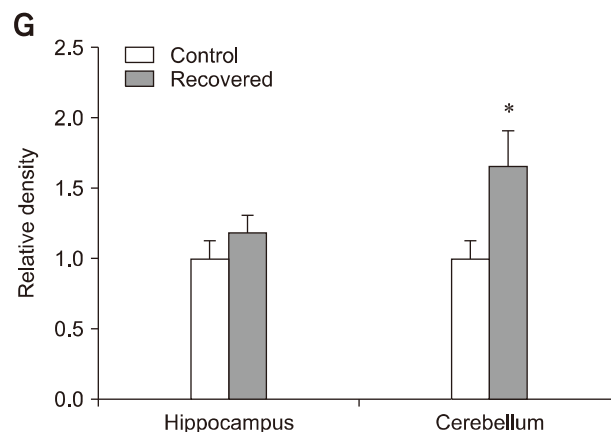

Fig. 4. Representative transmission electron microscopic photographs of the myelin sheath in control (A and C) and recovered (B and D) mice. Cross sections of myelinated axons are visible. The appearance and thickness of the myelin sheaths are comparable between the control and recovered mouse brain. Scale bars = 5 μm (A–D).

22% in the cerebellum. The increased G-ratio indicates that the thickness of the myelin sheath in the hippocampus and cerebellum of recovered mice significantly decreased, which suggests the presence of hypomyelination. This is because the G-ratio is defined as the ratio between the axonal radius (r) and fiber diameter (R), which is the sum of the axon diameter and the thickness of the myelin sheath (Fig. 5).

MBP expression in an OPC culture

An OPC culture was used to determine the effects of influenza infection on the expression of *MBP* in relation to proinflammatory cytokines. Prior to infection, the ratio of OPCs in the primary brain cell culture was measured by FACS. The average proportion of OPCs was 30.7%, which indicated that the primary brain cell culture was highly enriched with OPCs. The viabilities of the control and influenza-infected cultures measured for 48 h were 85.6% and 84.8%, respectively. The viability of both groups did not show any statistical difference at any assessment time (panel A in Fig. 6). *MBP* expression in the infected culture was significantly increased at 24 h ($p < 0.01$) and 48 h ($p < 0.05$; panel B in Fig. 6). The expression level of *IL-1β* in the infected culture started to increase from 12 h onward and showed a greater than 100-fold difference at 24 h ($p < 0.01$; panel C in Fig. 6). *TNF-α* expression in the infected culture showed a rapid increase as
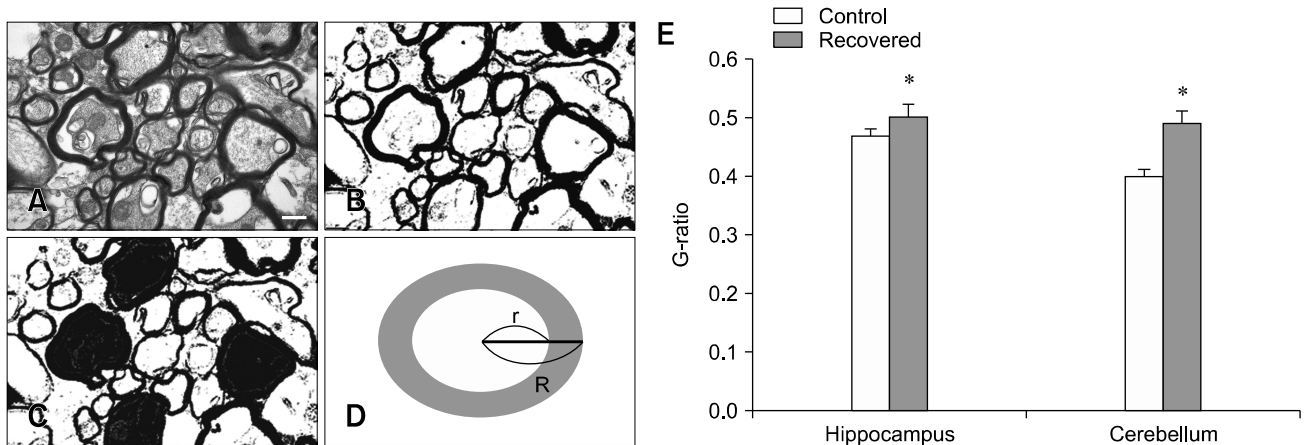
Fig. 5. A stepwise image conversion process to calculate the G-ratio. (A) An original image was converted to a black and white image by applying a threshold that would only reveal myelin sheaths. Scale bar = 5 μm. (B) Image analysis software was then used to obtain the area of the myelin sheath. (C) The areas that were occupied by axons were filled manually. The entire area occupied by the myelin sheaths and axons was then obtained. (D) Schematic representation (of an axon and myelin sheath) of how the G-ratio is obtained. By deducting the area occupied by the myelin sheaths from the entire area occupied by both the myelin sheaths and axons, the radius of the axons (r) and the thickness of the myelin sheaths (R − r) were obtained. The G-ratio was obtained by using the following formula: G = r/R. (E) A graph showing the G-ratio for the hippocampus and cerebellum. *$p < 0.05$.
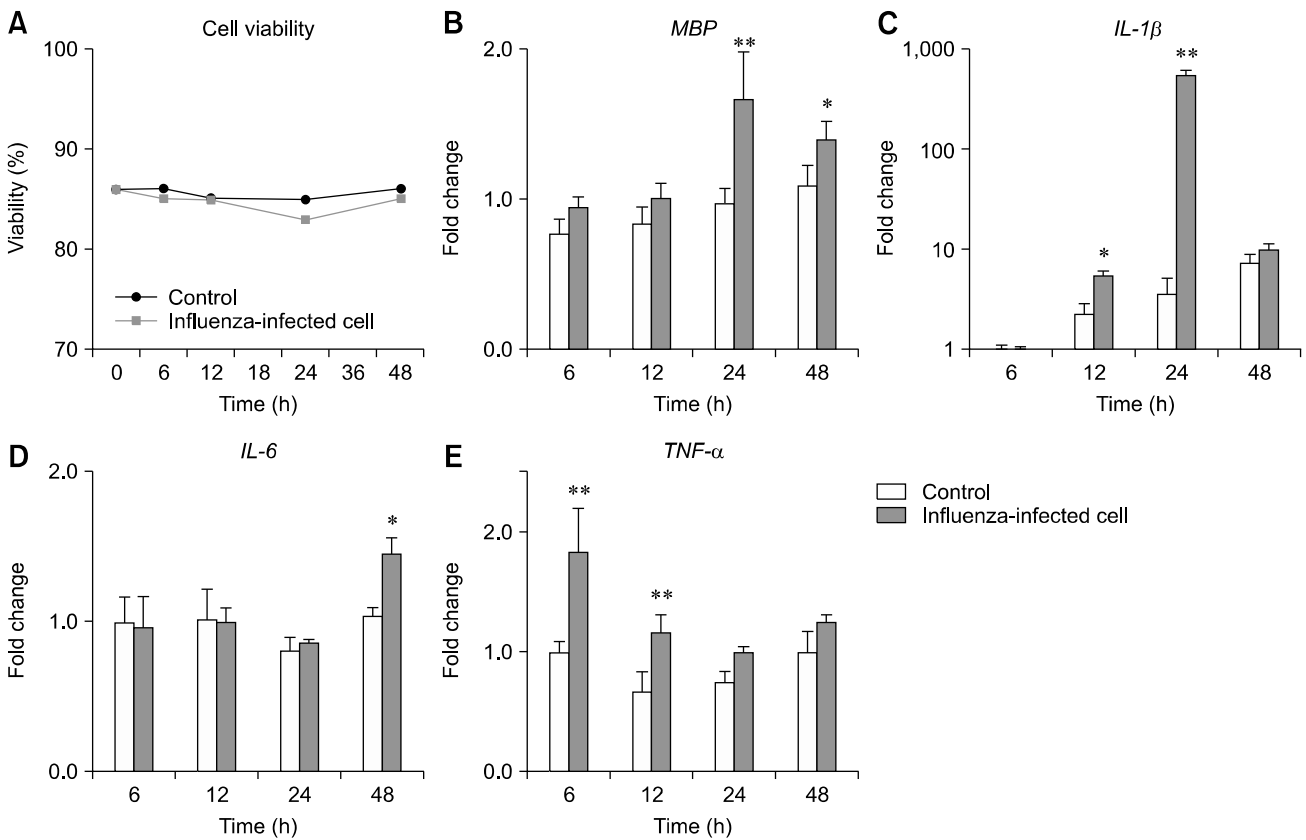

Fig. 6. (A) The viability of primary brain cell cultures enriched with oligodendrocyte precursor cells. Real-time polymerase chain reaction analysis of *myelin basic protein* (*MBP*; B), *interleukin-1β* (*IL-1β*; C), *interleukin-6* (*IL-6*; D), and *tumor necrosis factor-α* (*TNF-α*; E) expressions in control and influenza-infected cells (n = 6; *$p < 0.05$, **$p < 0.01$).

early as at 6 h and maintained the increase at 12 h ($p < 0.01$; panel E in Fig. 6). *IL-6* expression in the infected culture only showed a significant difference at 24 h after infection ($p < 0.05$; panel D in Fig. 6).

Discussion

The results showed that influenza infection induces long-term upregulation of MBP expression while decreasing the thickness of myelin sheaths surrounding axons in the cerebellum and hippocampus of influenza-recovered mice. Influenza infection may induce MBP expression by increasing proinflammatory cytokines without affecting oligodendrocyte viability. The results are in accordance with previous results which demonstrated that maternal influenza infection can cause changes in proteins associated with myelin formation in the offspring and can influence the effects of cytokines on MBP expression [6,18].

Many studies have been conducted to investigate the route and infection process of influenza in the CNS. Influenza viruses can infect the brain via the afferent nerve fibers upon intranasal inoculation [11,17,21,32]. During severe influenza infection, proinflammatory cytokines increase vascular hyperpermeability in the brain enabling the virus to enter brain parenchyma via the blood-brain barrier [5,28]. In addition, we recently reported that the influenza virus can infect the brain through the ventricles [34].

Upon influenza infection, the viruses are generally localized to certain areas of the brain. These areas include the substantia nigra, hippocampus, cerebellum, and brainstem [12,26]. The influenza virus infection is known to cause neuronal apoptosis and astrocyte activation in these areas [12,20,28]. We targeted the hippocampus and cerebellum in this experiment because these areas are prone to influenza virus infection, based on previous reports, and we recently observed that influenza infection can cause electrophysiological dysfunction in hippocampal neurons [22].

MBP accounts for about 30% of the proteins that make up the myelin sheath and is believed to be involved in myelin compaction [10]. Changes in MBP expression are associated with inflammatory responses [18]. Especially, TNF-α is known to induce proliferation of OPCs, which produce myelin [13,23,25]. Our observations from the OPC culture experiment further support previous results, as we observed that influenza infection increased MBP expression, which was preceded by TNF-α and IL-1β induction. In our previous study using a neonatal mouse infection model, we reported that the peak influenza infection was observed five days after infection. At the same time, increased release of proinflammatory cytokines such as TNF-α, IL-1β, and IL-6 were observed in the brain. Based on these results, the OPC culture system appears to well represent the *in vivo* infection model and is an effective method

to study oligodendrocyte function during infection.

Increased MBP expression after influenza infection could be explained by the effects of TNF-α and IL-1β. As TNF-α expression was induced in the early phase of infection, it potentially stimulated the proliferation of. A significant increase in IL-1β expression also supports the myelination process, as IL-1β expression induces ciliary neurotrophic factor expression in astrocytes, which is important for myelination [16]. However, it remains unclear why the thickness of myelin was reduced while MBP expression was increased in our study. As myelin is composed of many different proteins, there may be other components that could be adversely affected by the infection. Our preliminary microarray experiment did not reveal any downregulation of myelin-associated gene expression. Therefore, a potential explanation for the phenomenon is a delay in the remyelination process [19]. During the peak influenza infection period, many neurons and astrocytes undergo apoptosis followed by pathological changes in white matter [34]. It is expected that a compensatory increase in MBP expression takes place for remyelination while the repair process may take a longer time to achieve normal myelin thickness, as the translation and remyelination processes depend on various conditions.

In general, MBP mRNA and protein expressions have been observed by applying quantitative analytical methods; however, it was not possible to investigate the individual appearance of myelin sheaths in a quantitative manner. In contrast to a previous study that focused on changes in gene or protein expressions in relation to myelination, we attempted to evaluate changes in myelination properties by adopting the G-ratio concept [2,3]. Through this approach, we overcame the limitation of previous studies which were unable to quantify the properties of the myelin sheath based on ultrastructural changes. It should be noted that an increased G-ratio implies a decreased myelin thickness with a constant axon radius, and that condition is referred to as hypomyelination. Increases in the G-ratio in association with demyelination in have been reported in various diseases. Specifically, early influenza infection has been identified as a cause of depression and schizophrenia. Additionally, in patients with schizophrenia, an increased G-ratio has been reported [4,14,27]. Thus, our findings provide pathophysiological insights into the sequelae of early influenza infection.

We previously reported that hippocampal neurons from recovered mice failed to generate action potentials consistently upon repeated stimulation, and they showed lower neuronal excitability [22]. The results obtained from this study suggest that the neuronal dysfunction could be due to hypomyelination in influenza-recovered mice. It is generally accepted that hypomyelination affects neural conduction [24]. Therefore, our findings suggest that decreased hippocampal excitability in recovered mice could be due to hypomyelination caused by

influenza during a critical period of neural development. In conclusion, the present results have demonstrated that influenza infection during the neonatal period affects myelin expression and induces functional changes in the recovered mouse brain.

Acknowledgments

Conflicts of Interest

The authors declare no conflicts of interest.

References

1. **Baltagi SA, Shoykhet M, Felmet K, Kochanek PM, Bell MJ.** Neurological sequelae of 2009 influenza A (H1N1) in children: a case series observed during a pandemic. Pediatr Crit Care Med 2010, **11**, 179-184.

2. **Boullerne AI.** The history of myelin. Exp Neurol 2016, **283**, 431-445.

3. **Campbell JSW, Leppert IR, Narayanan S, Boudreau M, Duval T, Cohen-Adad J, Pike GB, Stikov N.** Promise and pitfalls of g-ratio estimation with MRI. Neuroimage 2018, **182**, 80-96.

4. **Chambers JS, Perrone-Bizzozero NI.** Altered myelination of the hippocampal formation in subjects with schizophrenia and bipolar disorder. Neurochem Res 2004, **29**, 2293-2302.

5. **Chaves AJ, Vergara-Alert J, Busquets N, Valle R, Rivas R, Ramis A, Darji A, Majó N.** Neuroinvasion of the highly pathogenic influenza virus H7N1 is caused by disruption of the blood brain barrier in an avian model. PLoS One 2014, **9**, e115138.

6. **Fatemi SH, Folsom TD, Reutiman TJ, Abu-Odeh D, Mori S, Huang H, Oishi K.** Abnormal expression of myelination genes and alterations in white matter fractional anisotropy following prenatal viral influenza infection at E16 in mice. Schizophr Res 2009, **112**, 46-53.

7. **Fatemi SH, Folsom TD, Reutiman TJ, Huang H, Oishi K, Mori S.** Prenatal viral infection of mice at E16 causes changes in gene expression in hippocampi of the offspring. Eur Neuropsychopharmacol 2009, **19**, 648-653.

8. **Goenka A, Michael BD, Ledger E, Hart IJ, Absoud M, Chow G, Lilleker J, Lunn M, McKee D, Peake D, Pysden K, Roberts M, Carrol ED, Lim M, Avula S, Solomon T, Kneen R.** Neurological manifestations of influenza infection in children and adults: results of a National British Surveillance Study. Clin Infect Dis 2014, **58**, 775-784.

9. **Ishida Y, Kawashima H, Morichi S, Yamanaka G, Okumura A, Nakagawa S, Morishima T.** Brain magnetic resonance imaging in acute phase of pandemic influenza A (H1N1) 2009 –associated encephalopathy in children. Neuropediatrics 2015, **46**, 20-25.

10. **Jahn O, Tenzer S, Werner HB.** Myelin proteomics: molecular anatomy of an insulating sheath. Mol Neurobiol 2009, **40**, 55-72.

11. **Jang H, Boltz D, Sturm-Ramirez K, Shepherd KR, Jiao Y, Webster R, Smeyne RJ.** Highly pathogenic H5N1 influenza virus can enter the central nervous system and induce neuroinflammation and neurodegeneration. Proc Natl Acad Sci USA 2009, **106**, 14063-14068.

12. **Kim M, Yu JE, Lee JH, Chang BJ, Song CS, Lee B, Paik DJ, Nahm SS.** Comparative analyses of influenza virus receptor distribution in the human and mouse brains. J Chem Neuroanat 2013, **52**, 49-57.

13. **Kıray H, Lindsay SL, Hosseinzadeh S, Barnett SC.** The multifaceted role of astrocytes in regulating myelination. Exp Neurol 2016, **283**, 541-549.

14. **Kneeland RE, Fatemi SH.** Viral infection, inflammation and schizophrenia. Prog Neuropsychopharmacol Biol Psychiatry 2013, **42**, 35-48.

15. **Kristensson K.** Avian influenza and the brain: comments on the occasion of resurrection of the Spanish flu virus. Brain Res Bull 2006, **68**, 406-413.

16. **Liberto CM, Albrecht PJ, Herx LM, Yong VW, Levison SW.** Pro-regenerative properties of cytokine-activated astrocytes. J Neurochem 2004, **89**, 1092-1100.

17. **Matsuda K, Park CH, Sunden Y, Kimura T, Ochiai K, Kida H, Umemura T.** The vagus nerve is one route of transneural invasion for intranasally inoculated influenza A virus in mice. Vet Pathol 2004, **41**, 101-107.

18. **McMurran CE, Jones CA, Fitzgerald DC, Franklin RJ.** CNS remyelination and the innate immune system. Front Cell Dev Biol 2016, **4**, 38.

19. **Michel K, Zhao T, Karl M, Lewis K, Fyffe-Maricich SL.** Translational control of myelin basic protein expression by ERK2 MAP kinase regulates timely remyelination in the adult brain. J Neurosci 2015, **35**, 7850-7865.

20. **Mori I, Kimura Y.** Apoptotic neurodegeneration induced by influenza A virus infection in the mouse brain. Microbes Infect 2000, **2**, 1329-1334.

21. **Park CH, Ishinaka M, Takada A, Kida H, Kimura T, Ochiai K, Umemura T.** The invasion routes of neurovirulent A/Hong Kong/483/97 (H5N1) influenza virus into the central nervous system after respiratory infection in mice. Arch Virol 2002, **147**, 1425-1436.

22. **Park H, Yu JE, Kim S, Nahm SS, Chung C.** Decreased Na$^+$ influx lowers hippocampal neuronal excitability in a mouse model of neonatal influenza infection. Sci Rep 2015, **5**, 13440.

23. **Patel JR, Williams JL, Muccigrosso MM, Liu L, Sun T, Rubin JB, Klein RS.** Astrocyte TNFR2 is required for CXCL12-mediated regulation of oligodendrocyte progenitor proliferation and differentiation within the adult CNS. Acta Neuropathol 2012, **124**, 847-860.

24. **Purger D, Gibson EM, Monje M.** Myelin plasticity in the central nervous system. Neuropharmacology 2016, **110**, 563-573.

25. **Rawji KS, Mishra MK, Yong VW.** Regenerative capacity of macrophages for remyelination. Front Cell Dev Biol 2016, **20**, 47.

26. **Takahashi M, Yamada T, Nakajima S, Nakajima K,**

Yamamoto T, Okada H. The substantia nigra is a major target for neurovirulent influenza A virus. J Exp Med 1995, **181**, 2161-2169.

27. **Walker CK, Roche JK, Sinha V, Roberts RC.** Substantia nigra ultrastructural pathology in schizophrenia. Schizophr Res 2018, **197**, 209-218.

28. **Wang S, Le TQ, Kurihara N, Chida J, Cisse Y, Yano M, Kido H.** Influenza virus-cytokine-protease cycle in the pathogenesis of vascular hyperpermeability in severe influenza. J Infect Dis 2010, **202**, 991-1001.

29. **Wilking AN, Elliott E, Garcia MN, Murray KO, Munoz FM.** Central nervous system manifestations in pediatric patients with influenza A H1N1 infection during the 2009 pandemic. Pediatr Neurol 2014, **51**, 370-376.

30. **Wong JY, Kelly H, Ip DK, Wu JT, Leung GM, Cowling BJ.** Case fatality risk of influenza A (H1N1pdm09): a systematic review. Epidemiology 2013, **24**, 830-841.

31. **Wu S, Wei Z, Greene CM, Yang P, Su J, Song Y, Iuliano AD, Wang Q.** Mortality burden from seasonal influenza and 2009 H1N1 pandemic influenza in Beijing, China, 2007-2013. Influenza Other Respir Viruses 2018, **12**, 88-97.

32. **Yamada M, Bingham J, Payne J, Rookes J, Lowther S, Haining J, Robinson R, Johnson D, Middleton D.** Multiple routes of invasion of wild-type Clade 1 highly pathogenic avian influenza H5N1 virus into the central nervous system (CNS) after intranasal exposure in ferrets. Acta Neuropathol 2012, **124**, 505-516.

33. **Yoganathan S, Sudhakar SV, James EJ, Thomas MM.** Acute necrotising encephalopathy in a child with H1N1 influenza infection: a clinicoradiological diagnosis and follow-up. BMJ Case Rep 2016, **2016**, bcr2015213429.

34. **Yu JE, Kim M, Lee J, Chang BJ, Song CS, Nahm SS.** Neonatal influenza infection causes pathological changes in the mouse brain. Vet Res 2014, **45**, 63.

35. **Zeng H, Quinet S, Huang W, Gan Y, Han C, He Y, Wang Y.** Clinical and MRI features of neurological complications after influenza A (H1N1) infection in critically ill children. Pediatr Radiol 2013, **43**, 1182-1189.